

# Study of chargino-neutralino production at hadron colliders in a long-lived slepton scenario

Ryuichiro Kitano

*Theoretical Division T-8, Los Alamos National Laboratory, Los Alamos, NM 87545*

## Abstract

The differential cross section of the chargino-neutralino production,  $q\bar{q} \rightarrow \chi^\pm \chi^0$ , followed by their decays into scalar tau leptons,  $\chi^\pm \chi^0 \rightarrow (\tilde{\tau}^\pm \nu)(\tilde{\tau}^\mp \tau^\pm) \rightarrow (\tilde{\tau}^\pm \nu)(\tilde{\tau}^\mp l^\pm \nu \bar{\nu})$ , is calculated with taking into account spin correlations. In the case where  $\tilde{\tau}$  is long-lived, this final state is fully reconstructable in a hadron-collider experiment up to a discrete two-fold ambiguity. Distributions of various kinematic variables can thus be observable and tell us about masses and spins of superparticles and also parity/CP violation in interactions by comparing with the cross-section formula. Observing non-trivial distributions derived in this paper will be a good test of supersymmetry.

# 1 Introduction

It is often stated that the LHC is a machine for discovery of new physics and we will need a new lepton collider to find out what it is. This is in many cases true because most of new physics signals at the LHC involve multiple jets in final states which are not simple objects to deal with. It is also true that studies of events with a missing momentum at hadron colliders are more challenging compared to ones at lepton colliders because we cannot balance the momentum in the beam direction. The unfixed energies of the initial partons are another obstacle in studying the exclusive processes. For this reason, most of studies are limited to a method to form a Lorentz (or a boost) invariant quantity out of visible objects and look for peaks, endpoints or excesses above expected backgrounds. That kind of observables are usually not enough information for us to reach to the Lagrangian.

Although lepton colliders generally offer a better environment for the studies of exclusive processes, it is not impossible at hadron colliders to carry out a detailed study of new-physics events if the final states are clean enough. In fact, one of the best-motivated models of new physics, supersymmetry (SUSY), may provide such an opportunity. In the case where the scalar tau lepton ( $\tilde{\tau}$ ) is lighter than the neutralinos and sufficiently long-lived, final states of SUSY events have two charged tracks of  $\tilde{\tau}$  rather than a missing momentum associated with escaping neutralinos. The presence of such a long-lived charged particle significantly improves the capability of the LHC study of SUSY models.

Although the light  $\tilde{\tau}$  scenario has been treated as an alternative and exotic possibility, it is actually neither theoretically exotic nor cosmologically problematic. Since the right-handed  $\tilde{\tau}$  carries only the  $U(1)_Y$  quantum number, the quantum correction to the mass is small in many models whereas colored and  $SU(2)$  charged sfermions obtain large positive contributions through diagrams with gauginos. In addition, the Yukawa interaction tends to give a negative contribution to the mass. Therefore, it is pretty reasonable to assume that  $\tilde{\tau}$  is the lightest among superpartners of the Standard Model fields. In such a case, the lifetime of  $\tilde{\tau}$  can be very long although the estimate depends on the detail of the model; it can decay into a gravitino and a tau lepton through a suppressed interaction if it is kinematically allowed or into two Standard Model fermions if the  $R$ -parity is violated. There are cosmological constraints on such a long-lived charged particle [1], but those can be evaded as long as we do not assume an extremely long lifetime. (See [2] for a recent realistic scenario of supersymmetry which predicts a long-lived  $\tilde{\tau}$  and naturally explains dark matter of the Universe by gravitinos.)

There have been studies of the long-lived  $\tilde{\tau}$  at the LHC, and dramatic differences from the stable neutralino scenario have been reported. In Ref. [3], a technique to reconstruct neutralino masses

has been proposed by looking for a decay process  $\chi^0 \rightarrow \tilde{\tau}\tau$ . (See [2, 4] for recent studies based on different SUSY models.) A detailed study of measuring the mass and the momentum of  $\tilde{\tau}$  in the muon system of the ATLAS detector has been done in Ref. [5, 6], and it was reported that the mass can be measured with an accuracy of  $O(0.1\%)$ . An amusing possibility to collect  $\tilde{\tau}$ 's by a material outside the detectors and measure its lifetime has been proposed in Refs. [7, 8, 9]. Recently, it was pointed out that the spin of  $\tilde{\tau}$  can be measured by looking at the angular distribution of the pair-production process of  $\tilde{\tau}$  [10].

In this paper, we study the production processes of neutralinos and charginos followed by their decays into  $\tilde{\tau}$ 's in the long-lived  $\tilde{\tau}$  scenario. We assume the lifetime of  $\tilde{\tau}$  is sufficiently long ( $\gg$  ns) so that most of the produced  $\tilde{\tau}$ 's reach to the muon system and their four-momentum can be measured. We mainly focus on the chargino-neutralino production process since it has the largest cross section and the final state is rather simple but rich enough to be reconstructed in the event-by-event basis. A particularly interesting process is  $q\bar{q} \rightarrow \chi^\pm\chi^0 \rightarrow (\tilde{\tau}^\pm\nu)(\tilde{\tau}^\mp\tau^\pm) \rightarrow (\tilde{\tau}^\pm\nu)(\tilde{\tau}^\mp l^\pm\nu\bar{\nu})$ , where it is required that the neutralino decays into  $\tilde{\tau}$  with the opposite charge to the one from the chargino to avoid a combinatorial background. The leptonically decaying  $\tau$ 's are selected so that we can easily measure the charge of  $\tau$ . The leptonic mode is also cleaner than  $\tau$ -jets with which we need to worry about uncertainties such as fake jets and the energy scale. The final state, two opposite-sign  $\tilde{\tau}$ 's, a lepton and a missing momentum, is clean enough to be compared directly with the theoretical calculation. We present a formula of the cross section with taking into account the spin correlations and demonstrate that various distributions can be seen at the LHC experiments. These distributions will be non-trivial tests of SUSY. Methods to measure the neutralino and chargino masses by using exclusive processes are also presented.

## 2 Interaction Lagrangian

There are two types of the Feynman diagrams for the  $\chi^\pm\chi^0$ -production process. One is through the  $s$ -channel  $W$ -boson exchange and the other is the  $t$ - and  $u$ -channel squark-exchange diagrams [11]. The interaction Lagrangian for the former diagram is

$$\mathcal{L}_W = \overline{\chi^0}\gamma^\mu(w_L P_L + w_R P_R)\chi^- W_\mu^+ + \text{h.c.}, \quad (1)$$

where  $w_L$  and  $w_R$  are coupling constants. We will discuss the relation to the fundamental parameters later. For the squark-exchange diagrams, the interaction terms are

$$\mathcal{L}_N = n_L^{(u)}(\overline{\chi^0}P_L u)\tilde{u}_L^\dagger + n_L^{(d)}(\overline{\chi^0}P_L d)\tilde{d}_L^\dagger + \text{h.c.}, \quad (2)$$

$$\mathcal{L}_C = c_L^{(u)}(\overline{\chi^+}P_L u)\tilde{d}_L^\dagger + c_L^{(d)}(\overline{\chi^+}P_L d)\tilde{u}_L^\dagger + \text{h.c.} \quad (3)$$

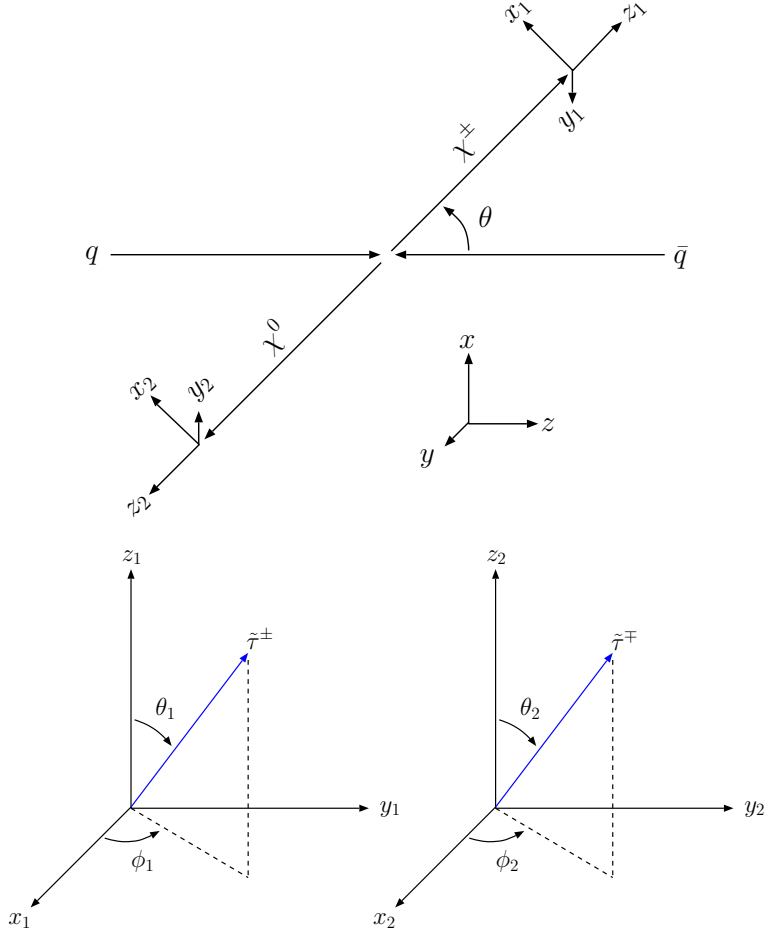


Figure 1: The coordinate systems.

If we neglect the  $u$ - and  $d$ -quark masses, there is no chargino coupling to the right-handed quarks. Therefore, only the left-handed (s)quarks participate in the diagrams.

The charginos decay through a term:

$$\mathcal{L}_{\chi^\pm}^D = c_L^{(\nu)} \overline{\chi^\pm} P_L \nu_\tau \tilde{\tau}^\dagger + \text{h.c.} \quad (4)$$

There are two terms for the neutralino decay:

$$\mathcal{L}_{\chi^0}^D = \overline{\chi^0} (n_R^{(\tau)} P_R + n_L^{(\tau)} P_L) \tau \tilde{\tau}^\dagger + \text{h.c.} \quad (5)$$

### 3 The cross-section formula

We calculate the differential cross section of  $q\bar{q} \rightarrow \chi^\pm \chi^0 \rightarrow (\tilde{\tau}^\pm \nu)(\tilde{\tau}^\mp \tau^\pm) \rightarrow (\tilde{\tau}^\pm \nu)(\tilde{\tau}^\mp l^\pm \nu \bar{\nu})$  in terms of the kinematic variables defined in Fig. 1. We require the neutralino to decay into  $\tilde{\tau}$  with the opposite charge to the chargino, and  $\tau$  to decay leptonically. By looking at the charges of the lepton and two  $\tilde{\tau}$ 's in the final state under this condition, we can tell which  $\tilde{\tau}$  is from the chargino. The angle  $\theta$  ( $0 \leq \theta \leq \pi$ ) is defined as the polar angle of the chargino momentum in the center-of-mass (CM) frame where we take the production plane to be the  $x$ - $z$  plane and the direction of the  $x$ -axis is chosen so that the  $x$ -component of the chargino momentum is positive. The direction of the  $z$ -axis is taken to be that of the  $q$  momentum. We also introduce angles  $\theta_1$  and  $\phi_1$  ( $\theta_2$  and  $\phi_2$ ) which are polar coordinates of the  $\tilde{\tau}^\pm$  ( $\tilde{\tau}^\mp$ ) momentum in the rest frame of  $\chi^\pm$  ( $\chi^0$ ) ( $0 \leq \theta_{1,2} \leq \pi$  and  $0 \leq \phi_{1,2} \leq 2\pi$ ). Momenta in those frames are related by the following Lorentz transformations:

$$p_{\text{CM}}^\mu = \begin{pmatrix} 1 & 0 & 0 & 0 \\ 0 & \cos \theta & 0 & \sin \theta \\ 0 & 0 & 1 & 0 \\ 0 & -\sin \theta & 0 & \cos \theta \end{pmatrix} \begin{pmatrix} \gamma_A & 0 & 0 & \gamma_A \beta_A \\ 0 & 1 & 0 & 0 \\ 0 & 0 & 1 & 0 \\ \gamma_A \beta_A & 0 & 0 & \gamma_A \end{pmatrix} p_1^\mu \quad (6)$$

$$= \begin{pmatrix} 1 & 0 & 0 & 0 \\ 0 & 1 & 0 & 0 \\ 0 & 0 & -1 & 0 \\ 0 & 0 & 0 & -1 \end{pmatrix} \begin{pmatrix} 1 & 0 & 0 & 0 \\ 0 & \cos \theta & 0 & -\sin \theta \\ 0 & 0 & 1 & 0 \\ 0 & \sin \theta & 0 & \cos \theta \end{pmatrix} \begin{pmatrix} \gamma_B & 0 & 0 & \gamma_B \beta_B \\ 0 & 1 & 0 & 0 \\ 0 & 0 & 1 & 0 \\ \gamma_B \beta_B & 0 & 0 & \gamma_B \end{pmatrix} p_2^\mu. \quad (7)$$

The boost factors are defined by

$$\gamma_A = \frac{1 + x_A^2 - x_B^2}{2x_A}, \quad \beta_A = \sqrt{1 - \frac{1}{\gamma_A^2}}, \quad (8)$$

$$\gamma_B = \frac{1 - x_A^2 + x_B^2}{2x_B}, \quad \beta_B = \sqrt{1 - \frac{1}{\gamma_B^2}}, \quad (9)$$

where  $x_A = m_{\chi^+}/\sqrt{\hat{s}}$  and  $x_B = m_{\chi^0}/\sqrt{\hat{s}}$  with  $\hat{s} = (P_{\chi^+} + P_{\chi^0})^2$ . For a later use, we here define

$$z_A \equiv 2x_A \gamma_A, \quad z_B \equiv 2x_B \gamma_B, \quad (10)$$

which are energies of the chargino and the neutralino in the CM frame normalized by  $\sqrt{\hat{s}}/2$ . Finally, we define

$$z_l \equiv \frac{E_l}{E_\tau}, \quad (0 \leq z_l \leq 1), \quad (11)$$

where energies of the lepton ( $E_l$ ) and  $\tau$  ( $E_\tau$ ) can be measured in any frame in the approximation of  $m_\tau \ll m_{\chi^0}$ . In this limit, the lepton momentum is pointing to the same direction as that of the parent  $\tau$ .

The cross-section formula can be written in terms of a product of density matrices of the production part  $\rho^{ab}$  and the decay parts  $D_A^a$  (chargino) and  $\tilde{D}_B^b$  (neutralino) ( $a, b = 0-3$ ). (See [12] for example for methods to calculate the cross section.) By using the narrow width approximation, it is given by

$$d\sigma = \frac{d \cos \theta}{2} \frac{d\Omega_1}{4\pi} \frac{d\Omega_2}{4\pi} dz_l \cdot \frac{1}{N_c} \frac{1}{16\pi} \frac{g_2^2}{2} \frac{z_A \beta_A}{\hat{s}} \left( \frac{1}{1 - x_W^2} \right)^2 \\ \times B(\chi^\pm \rightarrow \tilde{\tau}^\pm \nu) B(\chi^0 \rightarrow \tilde{\tau}^\mp \tau^\pm) B(\tau^\pm \rightarrow l^\pm \nu \bar{\nu}) \\ \times \sum_{a,b=0}^3 D_A^a(\theta_1, \phi_1) \rho^{ab}(\theta) \tilde{D}_B^b(\theta_2, \phi_2, z_l), \quad (12)$$

with

$$\tilde{D}_B^b(\theta_2, \phi_2, z_l) = \frac{1}{3}(1 - z_l) \left[ (5 + 5z_l - 4z_l^2) D_B^b(\theta_2, \phi_2) - a_N(1 + z_l - 8z_l^2) \delta^{b0} \right], \quad (13)$$

where  $g_2$  is the coupling constant of the  $SU(2)_L$  gauge interaction, and  $x_W = m_W/\sqrt{\hat{s}}$  with  $m_W$  being the  $W$ -boson mass. The delta factor is simply  $\delta^{b0} = (1, 0, 0, 0)$ . A real number  $a_N$  ( $-1 \leq a_N \leq 1$ ) represents parity violation in the  $\chi^0$ - $\tilde{\tau}$ - $\tau$  interaction:

$$a_N \equiv \frac{|n_L^{(\tau)}|^2 - |n_R^{(\tau)}|^2}{|n_L^{(\tau)}|^2 + |n_R^{(\tau)}|^2}. \quad (14)$$

Once we integrate out the lepton-energy fraction,  $z_l$ , the  $D_A \cdot \rho \cdot \tilde{D}_B$  part reduces to

$$D_A \cdot \rho \cdot \tilde{D}_B \rightarrow D_A \cdot \rho \cdot D_B. \quad (15)$$

The decay parts  $D_A^a$  and  $D_B^b$  have a simple form:

$$D_A^a = \begin{pmatrix} 1 \\ \pm a_C \sin \theta_1 \cos \phi_1 \\ \pm a_C \sin \theta_1 \sin \phi_1 \\ \pm a_C \cos \theta_1 \end{pmatrix}, \quad D_B^b = \begin{pmatrix} 1 \\ \mp a_N \sin \theta_2 \cos \phi_2 \\ \mp a_N \sin \theta_2 \sin \phi_2 \\ \mp a_N \cos \theta_2 \end{pmatrix}, \quad (16)$$

where  $a_C$  is the parity-violation factor in the chargino decay. It always takes the maximum value:

$$a_C = 1, \quad (17)$$

due to the fact that the neutrinos have only the left-handed chirality. Each component of  $D_A$  and  $D_B$  corresponds to a coefficient of expansions of the Hermitian  $2 \times 2$  spin-density matrices in terms of the unit ( $a, b = 0$ ) and the Pauli ( $a, b = 1-3$ ) matrices. The non-trivial dependencies on angles appear if there is parity violation in the decay vertices. An integration of a solid angle  $d\Omega_1$  ( $d\Omega_2$ ) leads to

$$D_A \cdot \rho \cdot \tilde{D}_B \rightarrow \rho^{0b} \cdot \tilde{D}_B, \quad (D_A \cdot \rho \cdot \tilde{D}_B \rightarrow D_A \cdot \rho^{a0} \tilde{D}_B^0). \quad (18)$$

When we perform a further integration of angles,  $d\Omega_1 d\Omega_2$ , and  $z_l$ , we obtain

$$D_A \cdot \rho \cdot \tilde{D}_B \rightarrow \rho^{00} \tilde{D}_B^0 \rightarrow \rho^{00}. \quad (19)$$

The production part  $\rho^{ab}$  is expressed in terms of  $\hat{s}$ , the angle  $\theta$  and effective coupling factors  $\bar{w}_L$  and  $\bar{w}_R$  defined by

$$\bar{w}_L \equiv w_L - \frac{1}{2} \frac{1 - x_W^2}{x_{\tilde{u}_L}^2 - \hat{t}/\hat{s}} \frac{c_L^{(u)} n_L^{(d)*}}{g_2/\sqrt{2}}, \quad (20)$$

$$\bar{w}_R \equiv w_R + \frac{1}{2} \frac{1 - x_W^2}{x_{\tilde{d}_L}^2 - \hat{u}/\hat{s}} \frac{c_L^{(d)*} n_L^{(u)}}{g_2/\sqrt{2}}, \quad (21)$$

where

$$\hat{t} = -\hat{s} z_A \cdot \frac{1 \mp \beta_A \cos \theta}{2}, \quad \hat{u} = -\hat{s} z_B \cdot \frac{1 \pm \beta_B \cos \theta}{2}, \quad (22)$$

and

$$x_{\tilde{u}_L} = \frac{m_{\tilde{u}_L}}{\sqrt{\hat{s}}}, \quad x_{\tilde{d}_L} = \frac{m_{\tilde{d}_L}}{\sqrt{\hat{s}}}. \quad (23)$$

The masses  $m_{\tilde{u}_L}$  and  $m_{\tilde{d}_L}$  are those of the left-handed squarks,  $\tilde{u}_L$  and  $\tilde{d}_L$ , respectively. The components  $\rho^{ab}$  are given by

$$\begin{aligned} \rho^{00} &= \frac{1}{4} (|\bar{w}_L|^2 + |\bar{w}_R|^2) z_A z_B (1 + \beta_A \beta_B \cos^2 \theta) \\ &\quad + 2 \text{Re}[\bar{w}_L^* \bar{w}_R] x_A x_B \\ &\quad \mp \frac{1}{2} (|\bar{w}_L|^2 - |\bar{w}_R|^2) z_A \beta_A \cos \theta, \end{aligned} \quad (24)$$

$$\begin{aligned} \rho^{01} &= \frac{1}{2} (|\bar{w}_L|^2 + |\bar{w}_R|^2) z_A x_B \sin \theta \\ &\quad + \text{Re}[\bar{w}_L^* \bar{w}_R] x_A z_B \sin \theta \\ &\quad \mp \frac{1}{2} (|\bar{w}_L|^2 - |\bar{w}_R|^2) z_A x_B \beta_A \cos \theta \sin \theta, \end{aligned} \quad (25)$$

$$\rho^{02} = \text{Im}[\bar{w}_L^* \bar{w}_R] x_A z_B \beta_B \sin \theta, \quad (26)$$

$$\begin{aligned} \rho^{03} &= \frac{1}{4} (|\bar{w}_L|^2 + |\bar{w}_R|^2) z_A z_B (1 + \beta_A \beta_B) \cos \theta \\ &\quad + 2 \text{Re}[\bar{w}_L^* \bar{w}_R] x_A x_B \cos \theta \\ &\quad \mp \frac{1}{4} (|\bar{w}_L|^2 - |\bar{w}_R|^2) z_A z_B (\beta_B + \beta_A \cos^2 \theta), \end{aligned} \quad (27)$$

$$\begin{aligned}
\rho^{10} &= \frac{1}{2}(|\bar{w}_L|^2 + |\bar{w}_R|^2)x_A z_B \sin \theta \\
&\quad + \text{Re}[\bar{w}_L^* \bar{w}_R] z_A x_B \sin \theta \\
&\quad \mp \frac{1}{2}(|\bar{w}_L|^2 - |\bar{w}_R|^2)x_A z_A \beta_A \cos \theta \sin \theta,
\end{aligned} \tag{28}$$

$$\begin{aligned}
\rho^{11} &= (|\bar{w}_L|^2 + |\bar{w}_R|^2)x_A x_B \sin^2 \theta \\
&\quad + \frac{1}{2}\text{Re}[\bar{w}_L^* \bar{w}_R] z_A z_B \sin^2 \theta,
\end{aligned} \tag{29}$$

$$\rho^{12} = -\frac{1}{2}\text{Im}[\bar{w}_L^* \bar{w}_R] z_A z_B \beta_B \sin^2 \theta, \tag{30}$$

$$\begin{aligned}
\rho^{13} &= \frac{1}{2}(|\bar{w}_L|^2 + |\bar{w}_R|^2)x_A z_B \cos \theta \sin \theta \\
&\quad + \text{Re}[\bar{w}_L^* \bar{w}_R] z_A x_B \cos \theta \sin \theta \\
&\quad \mp \frac{1}{2}(|\bar{w}_L|^2 - |\bar{w}_R|^2)x_A z_B \beta_B \sin \theta,
\end{aligned} \tag{31}$$

$$\rho^{20} = \text{Im}[\bar{w}_L^* \bar{w}_R] x_B z_A \beta_A \sin \theta, \tag{32}$$

$$\rho^{21} = \frac{1}{2}\text{Im}[\bar{w}_L^* \bar{w}_R] z_A z_B \beta_A \sin^2 \theta, \tag{33}$$

$$\rho^{22} = \frac{1}{2}\text{Re}[\bar{w}_L^* \bar{w}_R] z_A z_B \beta_A \beta_B \sin^2 \theta, \tag{34}$$

$$\rho^{23} = -\text{Im}[\bar{w}_L^* \bar{w}_R] z_A x_B \beta_A \cos \theta \sin \theta, \tag{35}$$

$$\begin{aligned}
\rho^{30} &= -\frac{1}{4}(|\bar{w}_L|^2 + |\bar{w}_R|^2)z_A z_B (1 + \beta_A \beta_B) \cos \theta \\
&\quad - 2\text{Re}[\bar{w}_L^* \bar{w}_R] x_A x_B \cos \theta \\
&\quad \pm \frac{1}{4}(|\bar{w}_L|^2 - |\bar{w}_R|^2)z_A z_B (\beta_A + \beta_B \cos^2 \theta),
\end{aligned} \tag{36}$$

$$\begin{aligned}
\rho^{31} &= -\frac{1}{2}(|\bar{w}_L|^2 + |\bar{w}_R|^2)z_A x_B \cos \theta \sin \theta \\
&\quad - \text{Re}[\bar{w}_L^* \bar{w}_R] x_A z_B \cos \theta \sin \theta \\
&\quad \pm \frac{1}{2}(|\bar{w}_L|^2 - |\bar{w}_R|^2)x_B z_A \beta_A \sin \theta,
\end{aligned} \tag{37}$$

$$\rho^{32} = \text{Im}[\bar{w}_L^* \bar{w}_R] z_B x_A \beta_B \cos \theta \sin \theta, \tag{38}$$

	C	P	T		C	P	T
$\cos \theta$	-	+	+	$a_W$	-	-	+
$\sin \theta$	+	+	+	$\xi_W$	+	+	+
$\cos \theta_{1,2}$	+	+	+	$\eta_W$	+	-	-
$\sin \theta_{1,2}$	+	+	+	$a_C$	-	-	+
$\cos \phi_{1,2}$	-	+	+	$a_N$	-	-	+
$\sin \phi_{1,2}$	-	-	-	$\pm$	-	+	+

Table 1: C, P, and T transformation properties of angles defined in Fig. 1, and those assigned for asymmetry parameters. With the assignments in the right table the interaction terms in the Lagrangian in Eqs. (1–5) recovers the C, P, and T symmetry. The symbol  $\pm$  represents the charge of the chargino.

$$\begin{aligned}
\rho^{33} = & -\frac{1}{4}(|\bar{w}_L|^2 + |\bar{w}_R|^2)z_A z_B (\beta_A \beta_B + \cos^2 \theta) \\
& -2\text{Re}[\bar{w}_L^* \bar{w}_R]x_A x_B \cos^2 \theta \\
& \pm \frac{1}{2}(|\bar{w}_L|^2 - |\bar{w}_R|^2)z_A \beta_A \cos \theta.
\end{aligned} \tag{39}$$

The energies  $z_A (\equiv 2E_{\chi^\pm} / \sqrt{\hat{s}})$  and  $z_B (\equiv 2E_{\chi^0} / \sqrt{\hat{s}})$  and the velocities  $\beta_A$  and  $\beta_B$  are constants with a fixed  $\hat{s}$  as defined in Eqs. (8), (9) and (10). The spin summed part  $\rho^{00}$  has been calculated in Ref. [11].

By using this cross-section formula we will be able to extract various information such as parity and CP violations of the interaction Lagrangian.

## 4 Angular and energy distributions

We can obtain various one-dimensional distributions by performing a phase-space integral in Eq. (12) while keeping a variable of interest a constant. In a simplified (and often realized) situation where the squark diagrams are not important, i.e., either squarks are heavy or one of the inos are Higgsino-like, we can obtain simple analytical expressions of distribution functions.

We list in Table 1 transformation properties of the angles under the charge conjugation (C), the parity transformation (P), and the time reversal (T). The transformation properties of asymmetry parameters are assigned in the right table ( $a_W$ ,  $\xi_W$ , and  $\eta_W$  will be defined later). With the assignments, the interaction terms in Eqs. (1–5) recovers the C, P, and T symmetry. These are helpful in understanding the distribution.

## $z_l$ distribution

The  $z_l$  distribution can be obtained without the simplification that squark diagrams are not important. By integrating  $\theta$ ,  $(\theta_1, \phi_1)$ , and  $(\theta_2, \phi_2)$ , we obtain

$$d\sigma = \sigma(q\bar{q} \rightarrow \chi^\pm \chi^0) B(\chi^\pm \rightarrow \tilde{\tau}^\pm \nu) B(\chi^0 \rightarrow \tilde{\tau}^\mp \tau^\pm) B(\tau^\pm \rightarrow l^\pm \nu \bar{\nu}) dz_l \times \frac{1}{3}(1 - z_l) [(5 + 5z_l - 4z_l^2) - a_N(1 + z_l - 8z_l^2)]. \quad (40)$$

This is the well-known polarization dependence of the lepton-energy distribution in the leptonic  $\tau$  decays [13]. Since  $z_l$  is a rotation and boost invariant quantity (in the limit of  $m_\tau/m_{\chi^0} \ll 1$ ), we can measure this distribution in the laboratory frame. This distribution will tell us about the parity asymmetry  $a_N$  in the neutralino decay through the  $\tau$  polarization.

## $\cos \theta_1$ distribution

By integrating  $\theta$ ,  $\phi_1$ ,  $(\theta_2, \phi_2)$ , and  $z_l$ , we obtain

$$d\sigma = \sigma(q\bar{q} \rightarrow \chi^\pm \chi^0) B(\chi^\pm \rightarrow \tilde{\tau}^\pm \nu) B(\chi^0 \rightarrow \tilde{\tau}^\mp \tau^\pm) B(\tau^\pm \rightarrow l^\pm \nu \bar{\nu}) \frac{d \cos \theta_1}{2} \times [1 + a_W a_C f_1(\beta_A, \beta_B) \cos \theta_1]. \quad (41)$$

Remember that  $a_C = 1$ . Explicit formulae of a function  $f_1$  and an asymmetry factor  $a_W$  can be derived in the simplified case where the squark diagrams are not important, i.e.,  $\bar{w}_L \simeq w_L$  and  $\bar{w}_R \simeq w_R$ :

$$f_1(\beta_A, \beta_B) = \frac{3\beta_A + \beta_B}{3 + \beta_A \beta_B + 3\xi_W \sqrt{(1 - \beta_A^2)(1 - \beta_B^2)}}, \quad (42)$$

and

$$a_W = \frac{|w_L|^2 - |w_R|^2}{|w_L|^2 + |w_R|^2}, \quad \xi_W = \frac{2\text{Re}[w_L^* w_R]}{|w_L|^2 + |w_R|^2}. \quad (43)$$

Even though  $\cos \theta_1$  is P-even (see Table 1), this distribution looks at parity violation in the production process  $a_W$  by picking up another parity violation in the chargino decay  $a_C$ .

In hadron collisions, event rates are obtained after convoluting with the parton distribution functions. The actual distribution we will see is  $\propto 1 + a_W \langle f_1 \rangle \cos \theta_1$  where  $\langle f_1 \rangle$  is an averaged value of  $f_1$ . The value of  $f_1$  vanishes in the threshold production limit ( $\beta_A \rightarrow 0$ ,  $\beta_B \rightarrow 0$ ), and it approaches to unity for a boosted event ( $\beta_A \rightarrow 1$ ,  $\beta_B \rightarrow 1$ ). A larger asymmetry can be observed if we select events with large  $\hat{s}$  although the number of events exponentially fall off with the imposed lower cut on  $\hat{s}$ . Observing this asymmetry will be an evidence of the chargino spin and parity violation in the weak interaction of inos.

## cos $\theta_2$ distribution

A similar distribution is obtained when we integrate  $\theta$ ,  $(\theta_1, \phi_1)$ ,  $\phi_2$ , and  $z_l$ :

$$d\sigma = \sigma(q\bar{q} \rightarrow \chi^\pm \chi^0) B(\chi^\pm \rightarrow \tilde{\tau}^\pm \nu) B(\chi^0 \rightarrow \tilde{\tau}^\mp \tau^\pm) B(\tau^\pm \rightarrow l^\pm \nu \bar{\nu}) \frac{d \cos \theta_2}{2} \times [1 + a_W a_N f_1(\beta_B, \beta_A) \cos \theta_2]. \quad (44)$$

The angular dependence is made possible by the neutralino spin and it measures the parity violations in the production and the decay.

## cos $\theta_1$ cos $\theta_2$ distribution

A non-trivial correlation is present between angles in both sides of decays. The  $\theta_1$  and  $\theta_2$  dependence of the cross section is

$$d\sigma = \sigma(q\bar{q} \rightarrow \chi^\pm \chi^0) B(\chi^\pm \rightarrow \tilde{\tau}^\pm \nu) B(\chi^0 \rightarrow \tilde{\tau}^\mp \tau^\pm) B(\tau^\pm \rightarrow l^\pm \nu \bar{\nu}) \frac{d \cos \theta_1}{2} \frac{d \cos \theta_2}{2} \times [1 + a_W a_C f_1(\beta_A, \beta_B) \cos \theta_1 + a_W a_N f_1(\beta_B, \beta_A) \cos \theta_2 + a_C a_N f_2(\beta_A, \beta_B) \cos \theta_1 \cos \theta_2], \quad (45)$$

where

$$f_2(\beta_A, \beta_B) = \frac{3\beta_A \beta_B + 1 + \xi_W \sqrt{(1 - \beta_A^2)(1 - \beta_B^2)}}{3 + \beta_A \beta_B + 3\xi_W \sqrt{(1 - \beta_A^2)(1 - \beta_B^2)}}. \quad (46)$$

Integrating  $\theta_1$  and  $\theta_2$  while keeping a product  $\cos \theta_1 \cos \theta_2 (\equiv y)$  constant, we obtain

$$d\sigma = \sigma(q\bar{q} \rightarrow \chi^\pm \chi^0) B(\chi^\pm \rightarrow \tilde{\tau}^\pm \nu) B(\chi^0 \rightarrow \tilde{\tau}^\mp \tau^\pm) B(\tau^\pm \rightarrow l^\pm \nu \bar{\nu}) \frac{dy}{2} \times [1 + a_C a_N f_2(\beta_A, \beta_B) y] \log |y|. \quad (47)$$

The non-trivial part (the second term) is due to spin correlations of the chargino and the neutralino in the intermediate states. Parity violation,  $a_N \neq 0$ , biases the distribution towards a positive or negative value of  $y$ . This distribution is independent of the asymmetry in the production process,  $a_W$ . Note also that the function  $f_2$  does not vanish in the limit of the threshold production although it is maximized in the boost limit. Confirming this correlation will be an interesting test of the model.

## $\phi_1$ distribution

A non-trivial distribution of the azimuthal angle  $\phi_1$  takes place due to parity violation in the chargino decay:

$$d\sigma = \sigma(q\bar{q} \rightarrow \chi^\pm \chi^0) B(\chi^\pm \rightarrow \tilde{\tau}^\pm \nu) B(\chi^0 \rightarrow \tilde{\tau}^\mp \tau^\pm) B(\tau^\pm \rightarrow l^\pm \nu \bar{\nu}) \frac{d\phi_1}{2\pi} \\ \times \left[ 1 \pm \frac{\pi^2}{16} a_C g_1(\beta_A, \beta_B) \cos \phi_1 \pm \frac{\pi^2}{16} a_C \eta_W g_2(\beta_A, \beta_B) \sin \phi_1 \right], \quad (48)$$

where

$$g_1(\beta_A, \beta_B) = \frac{\sqrt{1 - \beta_A^2} + \xi_W \sqrt{1 - \beta_B^2}}{1 + \beta_A \beta_B / 3 + \xi_W \sqrt{(1 - \beta_A^2)(1 - \beta_B^2)}}, \quad (49)$$

$$g_2(\beta_A, \beta_B) = \frac{\beta_A \sqrt{1 - \beta_B^2}}{1 + \beta_A \beta_B / 3 + \xi_W \sqrt{(1 - \beta_A^2)(1 - \beta_B^2)}}. \quad (50)$$

The  $\phi_1$  dependence appears even if  $a_W = 0$ . This is somewhat surprising once we realize the fact that  $\cos \phi_1$  is P-even and we have already picked up a parity violation in the chargino decay ( $a_C$ ). In order to be consistent with the parity-transformation property, there should be another parity violation. This is in fact supplied by maximal parity violation in the weak interaction of quarks in the production process. This means that one needs to measure the direction of the quark (or the anti-quark) to observe or to even define this distribution. The difference of the signs for the  $\chi^+ \chi^0$  and  $\chi^- \chi^0$  productions can be understood by the fact that  $\cos \phi_1$  and  $\sin \phi_1$  are CPT-odd. The  $\sin \phi_1$  dependence (phase of the  $\phi_1$  oscillation) measures CP (or T) violation in the production process:

$$\eta_W = \frac{2\text{Im}[w_L^* w_R]}{|w_L|^2 + |w_R|^2}. \quad (51)$$

The function  $g_1$  is maximized at the threshold limit, and vanishes in the boost limit in contrast to the case of the polar-angle dependencies. In the threshold limit, the coefficient of  $\cos \phi_1$  is  $\pi^2/16$ . The CP asymmetry vanishes in both the threshold and the boost limits.

The determination of the spin of the intermediate particles by looking at the azimuthal-angle distributions (frequencies of the  $\phi$  oscillations) has been discussed recently in Ref. [14]\*.

---

\*As we have seen above, we need parity violation in *both* the production and the decay vertices in order to develop this azimuthal-angle dependence. This is true for processes of  $2 \rightarrow 2$  fermion productions and their two-body decays. Therefore, the method of Ref. [14] should work in a limited case. For example, there would not be the azimuthal-angle dependence in processes with QED or QCD productions of fermions such as the production of a  $t\bar{t}$  pair and a gluino pair at hadron colliders (unless the beam is polarized). In such processes, the angular correlations between two decays such as the distribution of  $\cos \theta_1 \cos \theta_2$  or  $\phi_1 \pm \phi_2$  will instead be useful if there is parity violation in the decay vertices.

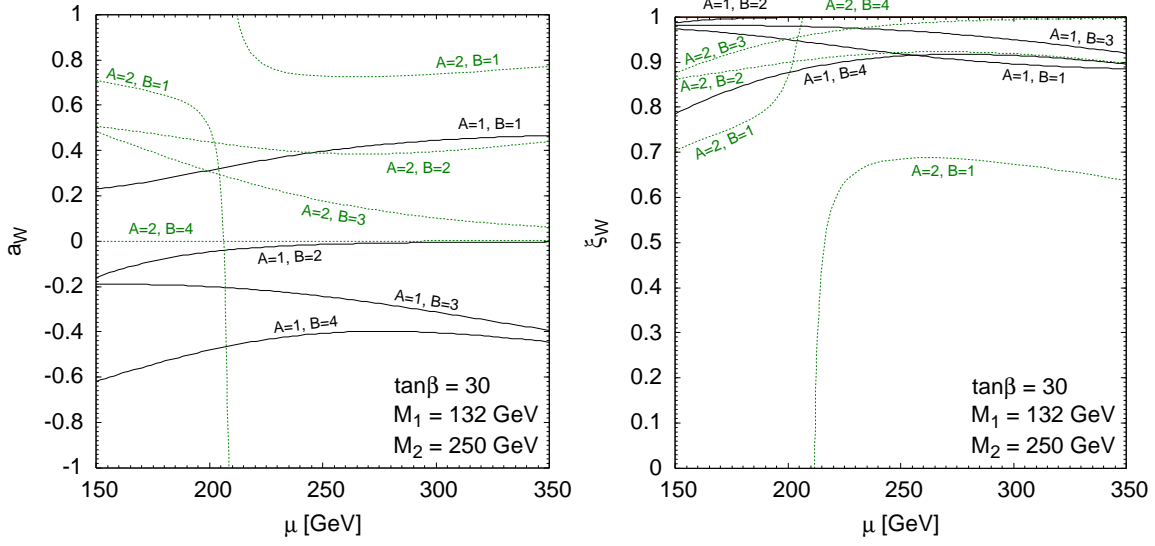


Figure 2: The  $\mu$  parameter dependence of  $a_W$  and  $\xi_W$ . The labels  $A = 1, 2$  and  $B = 1 - 4$  represent each mass eigenstate of the charginos and the neutralinos.

### $\phi_2$ distribution

A similar distribution is obtained when  $a_N$  is non-vanishing:

$$\begin{aligned}
 d\sigma &= \sigma(q\bar{q} \rightarrow \chi^\pm \chi^0) B(\chi^\pm \rightarrow \tilde{\tau}^\pm \nu) B(\chi^0 \rightarrow \tilde{\tau}^\mp \tau^\pm) B(\tau^\pm \rightarrow l^\pm \nu\bar{\nu}) \frac{d\phi_2}{2\pi} \\
 &\times \left[ 1 \mp \frac{\pi^2}{16} a_N g_1(\beta_B, \beta_A) \cos \phi_2 \mp \frac{\pi^2}{16} a_N \eta_W g_2(\beta_B, \beta_A) \sin \phi_2 \right]. \quad (52)
 \end{aligned}$$

### Other distributions

Although we will not study in this paper, there are various kinds of other non-trivial distributions. For example, the distribution of the difference of the angles  $\phi_1 - \phi_2$  also depends on the CP-violation parameter  $\eta_W$ . In the reconstruction of this angle at hadron colliders we do not need to know the direction of  $q$  or  $\bar{q}$  in the initial state in contrast to the case of the angles  $\phi_1$  and  $\phi_2$ . This is an advantage especially at  $pp$  colliders although the analytic expression of the distribution is slightly complicated.

## 5 Asymmetries vs parameters in the Lagrangian

In this section, we discuss model parameters and their relations to the observables such as  $a_N$ ,  $a_W$  and  $\eta_W$ . There are five model parameters which are relevant for the process: the Higgsino mass

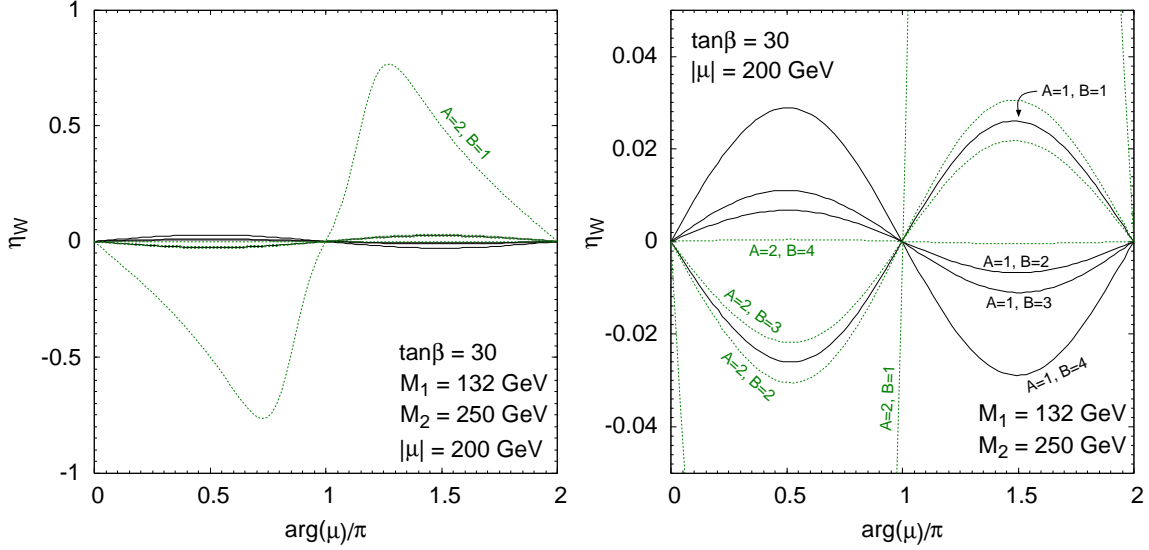


Figure 3: The phase dependence of the CP asymmetry  $\eta_W$ . The right figure is the same as the left figure with a different scale.

parameter  $\mu$ , the ratio of the vacuum expectation values of the Higgs fields  $\tan\beta (\equiv \langle H_2 \rangle / \langle H_1 \rangle)$ , the gaugino mass parameters  $M_1$  and  $M_2$ , and the mixing parameter of the scalar tau leptons  $\theta_{\tilde{\tau}}$  ( $\tilde{\tau}_1 = \cos\theta_{\tilde{\tau}}\tilde{\tau}_R + \sin\theta_{\tilde{\tau}}\tilde{\tau}_L$ ).

The coupling constants  $w_{L,R}$  and  $n_{L,R}^{(\tau)}$  in Eqs. (1) and (5) are expressed in terms of mixing matrices of the neutralinos  $O_N$ , of the charginos  $O_L$  and  $O_R$ , and the mixing angle of the scalar tau leptons  $\theta_{\tilde{\tau}}$ :

$$w_L = g_2(O_N^*)_{B2}(O_L^*)_{A1} + \frac{g_2}{\sqrt{2}}(O_N^*)_{B3}(O_L^*)_{A2}, \quad (53)$$

$$w_R = g_2(O_N)_{B2}(O_R^*)_{A1} - \frac{g_2}{\sqrt{2}}(O_N)_{B4}(O_R^*)_{A2}, \quad (54)$$

and

$$n_L^{(\tau)} = -\frac{g_2}{\sqrt{2}}(O_N)_{B2} \sin\theta_{\tilde{\tau}} - \frac{g_Y}{\sqrt{2}}(O_N)_{B1} \sin\theta_{\tilde{\tau}} - \frac{m_\tau}{v \cos\beta}(O_N)_{B3} \cos\theta_{\tilde{\tau}}, \quad (55)$$

$$n_R^{(\tau)} = \sqrt{2}g_Y(O_N^*)_{B1} \cos\theta_{\tilde{\tau}} - \frac{m_\tau}{v \cos\beta}(O_N^*)_{B3} \sin\theta_{\tilde{\tau}}, \quad (56)$$

where  $g_Y$  is the coupling constant of the  $U(1)_Y$  gauge interaction. The mixing matrices are defined by

$$O_N M_{\chi^0} O_N^T = M_{\chi^0}^{\text{diag.}}, \quad (57)$$

$$O_R M_{\chi^+} O_L^\dagger = M_{\chi^+}^{\text{diag.}}, \quad (58)$$

where the right-hand-side of the equations are diagonal matrices with real and positive eigenvalues. The mass matrices  $M_{\chi^0}$  and  $M_{\chi^\pm}$  are

$$M_{\chi^0} = \begin{pmatrix} M_1 & 0 & \frac{g_Y v}{\sqrt{2}} \cos \beta & -\frac{g_Y v}{\sqrt{2}} \sin \beta \\ 0 & M_2 & -\frac{g_2 v}{\sqrt{2}} \cos \beta & \frac{g_2 v}{\sqrt{2}} \sin \beta \\ \frac{g_Y v}{\sqrt{2}} \cos \beta & -\frac{g_2 v}{\sqrt{2}} \cos \beta & 0 & -\mu \\ -\frac{g_Y v}{\sqrt{2}} \sin \beta & \frac{g_2 v}{\sqrt{2}} \sin \beta & -\mu & 0 \end{pmatrix}, \quad (59)$$

and

$$M_{\chi^\pm} = \begin{pmatrix} M_2 & -g_2 v \cos \beta \\ -g_2 v \sin \beta & \mu \end{pmatrix}. \quad (60)$$

The vacuum expectation value  $v$  is  $v = \sqrt{\langle H_1 \rangle^2 + \langle H_2 \rangle^2} = 174$  GeV.

We show in Fig. 2 the  $a_W$  and  $\xi_W$  factors in a limited case where we fix  $(\tan \beta, M_1, M_2)$  to be  $(30, 132$  GeV,  $250$  GeV) and vary the  $\mu$  parameter from  $150$  GeV to  $350$  GeV. The labels  $A = 1, 2$  and  $B = 1 - 4$  represent each mass eigenstate of the charginos and the neutralinos, respectively. Various values can be obtained, but the largest cross section is for  $A = 1$  and  $B = 2$  which gives  $a_W \simeq 0$  and  $\xi_W \simeq 1$ .

The CP asymmetry  $\eta_W$  is calculated with varying the phase of the  $\mu$  parameter in Fig. 3. The parameters are fixed as  $(\tan \beta, M_1, M_2, |\mu|) = (30, 132$  GeV,  $250$  GeV,  $200$  GeV). A large CP asymmetry is obtained only for  $A = 2$  and  $B = 1$ . Others are at most of order a few percent. (The relative phase between  $M_1$  and  $M_2$  is also physical.)

Finally, the parity asymmetry  $a_N$  in the neutralino decay is calculated with  $(\tan \beta, M_1, M_2) = (30, 132$  GeV,  $250$  GeV) in Fig. 4. We take three values of the  $\tilde{\tau}$ -mixing parameter  $\theta_{\tilde{\tau}} = 0, \pi/4, \pi/2$ . It shows that  $a_N$  has rich information on model parameters, i.e., nature of the neutralino and  $\tilde{\tau}$ .

## 6 LHC studies of $\chi^+ \chi^-$ and $\chi^\pm \chi^0$ productions

In this section, we demonstrate a possible strategy for the study of the production processes of charginos and neutralinos by using a Monte Carlo simulation. We use the following simplified model for generating events:

$$\mu = 300 \text{ GeV}, \quad M_1 = M_2 = m_{\tilde{u}_L} = m_{\tilde{d}_L} = 5000 \text{ GeV}, \quad (61)$$

$$\tan \beta = 10, \quad m_{\tilde{\tau}_L} = 5000 \text{ GeV}, \quad m_{\tilde{\tau}_R} = 100 \text{ GeV}. \quad (62)$$

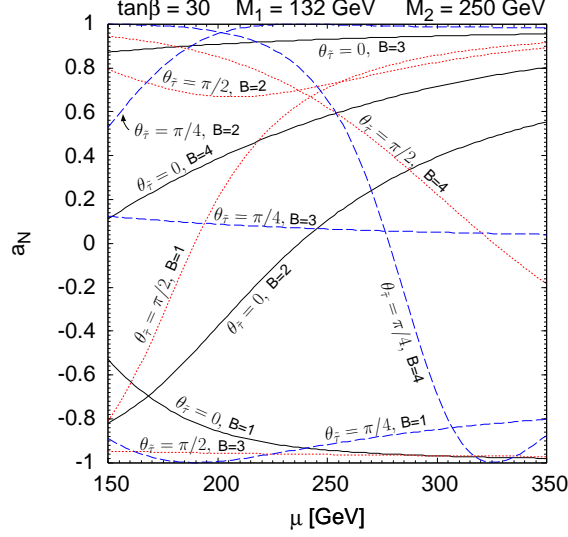


Figure 4: The  $\mu$  parameter dependence of the parity asymmetry  $a_N$ .

With this choice of parameters, all the SUSY particles decouple from low energy except for the Higgsinos and the right-handed  $\tilde{\tau}$ . The chargino and two light neutralinos are purely Higgsino-like and masses are calculated to be:

$$m_{\tilde{\tau}_1} = 109 \text{ GeV}, \quad m_{\chi_1^+} = 300 \text{ GeV}, \quad m_{\chi_1^0} = 299 \text{ GeV}, \quad m_{\chi_2^0} = 301 \text{ GeV}. \quad (63)$$

Although there are two mass eigenstates for the neutralinos due to a small mixing with gauginos, they almost behave like a single Dirac fermion. We do not distinguish  $\chi_1^0$  and  $\chi_2^0$  in the following analysis. The lifetime of  $\tilde{\tau}_1$  is assumed to be much longer than the typical collider time scale ( $1/\Gamma_{\tilde{\tau}} \gg \text{ns}$ ). The branching fractions of the chargino and the neutralino decays are of course,

$$B(\chi^\pm \rightarrow \tilde{\tau}^\pm \nu) \simeq 1.0, \quad B(\chi^0 \rightarrow \tilde{\tau}^\pm \tau^\mp) \simeq 0.5. \quad (64)$$

The asymmetry parameters in this model are calculated to be

$$a_N = 1.00, \quad a_W = 0.00, \quad \xi_W = 1.00, \quad \eta_W = 0.00. \quad (65)$$

We have generated 26,000 events of the electroweak production processes of SUSY particles (including the  $\tilde{\tau}$  pair-production process) in the  $pp$  collision at  $\sqrt{s} = 14 \text{ TeV}$  by using the Herwig 6.5 event generator [15]. The spin correlations have been implemented for the  $\chi^+ \chi^0$  production and their decays [16, 17]. This number of events corresponds to an integrated luminosity of  $100 \text{ fb}^{-1}$  at the LHC. (We will use  $300 \text{ fb}^{-1}$  of data for some of the analysis of angular distributions.) We have used the CTEQ5L library [18] for the parton distribution function. For the  $\tau$  decay, we have

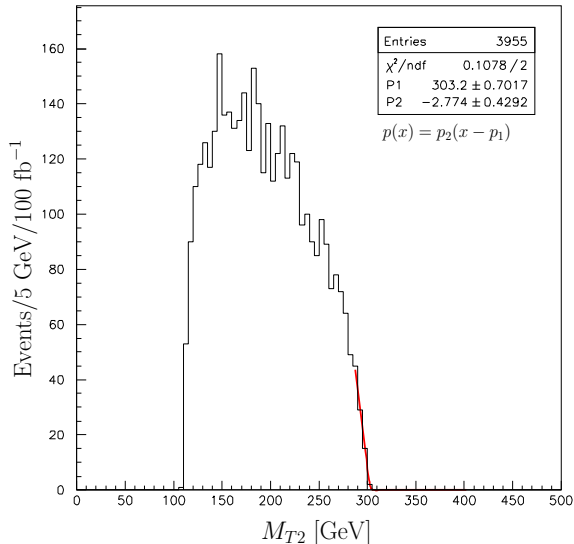


Figure 5: The  $M_{T2}$  distribution of the chargino-pair production. The chargino mass can be extracted by looking at the endpoint.

used TAUOLA 2.7 package [19] so that the spin information is maintained. A detector simulator AcerDET 1.0 [20] has been used for the event analysis.

In the following analysis, we assume that the mass of  $\tilde{\tau}$  is known by the method of Ref. [6], and we ignore the resolution of the  $\tilde{\tau}$ -momentum measurements which is of order a few percent in the ATLAS experiment [5]. One should note that the accuracies of the measurement quoted below are somewhat optimistic for this reason. We also assume perfect efficiencies of the  $\tilde{\tau}$  identification and of the  $\tilde{\tau}$ -charge measurement for  $\tilde{\tau}$  tracks with  $p_T > 10$  GeV and  $|\eta| < 2.5$ . By requiring two  $\tilde{\tau}$ 's, there is no Standard Model background with this assumption although one needs to take into account mis-identifications of muons as  $\tilde{\tau}$  in actual experiments.

We first discuss possible methods to measure the masses of the chargino and the neutralino through the exclusive production processes. Measurements of the asymmetries by looking at the angular and energy distributions studied in Section 4 will then be demonstrated.

## 6.1 Chargino mass determination by chargino-pair production

We present a method to measure the chargino mass exclusively from the chargino pair-production process. The final state of the process is two opposite-sign  $\tilde{\tau}$ 's and a missing momentum by two neutrinos.

Although we cannot reconstruct the chargino momentum in the event-by-event basis, an end-

point analysis developed in Ref. [21] can be used to extract the chargino mass. The method is to form a quantity  $M_{T2}$  defined by

$$M_{T2}^2 = \min_{\mathbf{p}_{T\nu_1} + \mathbf{p}_{T\nu_2} = \mathbf{p}_T^{\text{miss}}} [\max\{m_T^2(\mathbf{p}_{T\tilde{\tau}^-}, \mathbf{p}_{T\nu_1}), m_T^2(\mathbf{p}_{T\tilde{\tau}^+}, \mathbf{p}_{T\nu_2})\}], \quad (66)$$

where  $\mathbf{p}_{T\tilde{\tau}^-}$  and  $\mathbf{p}_{T\tilde{\tau}^+}$  are the transverse momentum of the two  $\tilde{\tau}$ 's and  $\mathbf{p}_T^{\text{miss}}$  is the missing transverse momentum. The transverse mass  $m_T$  is defined by

$$\begin{aligned} m_T^2 &= (E_{T\tilde{\tau}} + E_{T\nu})^2 - |\mathbf{p}_{T\tilde{\tau}} + \mathbf{p}_{T\nu}|^2 \\ &= m_{\tilde{\tau}}^2 + 2(E_{T\tilde{\tau}}E_{T\nu} - \mathbf{p}_{T\tilde{\tau}} \cdot \mathbf{p}_{T\nu}), \end{aligned} \quad (67)$$

where

$$E_T^2 = m^2 + |\mathbf{p}_T|^2. \quad (68)$$

The quantity  $M_{T2}$  is designed to have an endpoint at the mass of the intermediate particle.

In order to select the  $\chi^+\chi^-$  events, we have imposed a jet and a lepton vetoes:

$$N_{\tilde{\tau}^+} = N_{\tilde{\tau}^-} = 1, \quad N_j(p_T > 30 \text{ GeV}) = 0, \quad N_l(p_T > 6 \text{ GeV}) = 0. \quad (69)$$

We do not need to impose a tight cut on a missing momentum since  $\tilde{\tau}^+\tilde{\tau}^-$  events do not contribute near the endpoint of the distribution. The  $M_{T2}$  distribution is shown in Fig. 5. There is a clear endpoint around the input chargino mass, 300 GeV. By fitting with a linear function, we obtain the endpoint:  $303.2 \pm 0.7$  GeV, which is slightly larger than the input value due to the resolution of the missing transverse momentum.

## 6.2 Neutralino and chargino mass determination by chargino-neutralino production

We show in this subsection that quite accurate measurements of the neutralino and chargino masses are possible by the analysis of the exclusive processes. Combining various methods described below, we will be able to measure the masses at the level of a few GeV.

### 6.2.1 Endpoint analysis for the neutralino mass

The neutralino mass can be measured by looking for an endpoint of the invariant mass distribution of the  $\tilde{\tau}^\mp l^\pm$  pair from the neutralino decay followed by the leptonic tau decay. The  $\chi^\pm\chi^0$ -production process can be selected by requiring two  $\tilde{\tau}$ 's and an isolated lepton:

$$N_{\tilde{\tau}^+} = N_{\tilde{\tau}^-} = 1, \quad N_j(p_T > 30 \text{ GeV}) = 0, \quad N_l(p_T > 10 \text{ GeV}) = 1. \quad (70)$$

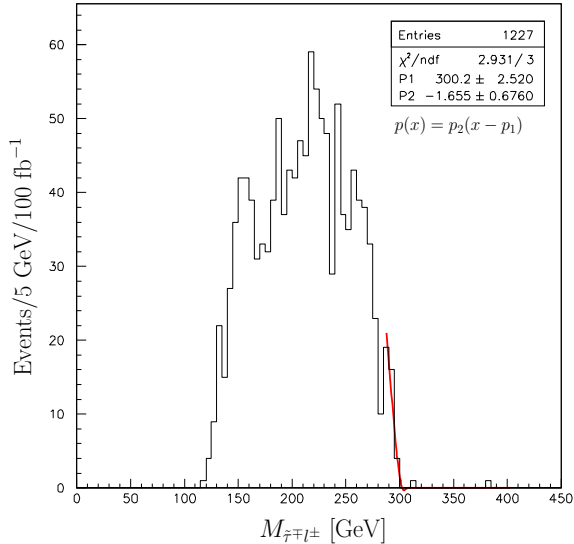


Figure 6: Invariant mass distribution of  $\tilde{\tau}^\mp l^\pm$  pairs. The endpoint shows the neutralino mass.

As we discussed before, we require that two  $\tilde{\tau}$ 's have opposite signs so that there is no ambiguity in selecting  $\tilde{\tau}$  from the neutralino decay.

The invariant mass distribution of the  $\tilde{\tau}^\mp l^\pm$  pair is shown in Fig. 6. An accurate measurement of the neutralino mass is possible by this method ( $300 \pm 3$  GeV).

### 6.2.2 Solvability analysis for the neutralino mass

By using the information of the chargino mass measured by the  $\chi^+ \chi^-$  pair production process, we can obtain the neutralino mass by a similar method proposed in Refs. [22, 23]. (See also [24] for a similar analysis for the measurement of the top-quark mass in the di-lepton events from the  $t\bar{t}$  productions at the LHC.) Since the final state is relatively simple, we can solve the kinematics in the event-by-event basis by postulating a neutralino mass. By maximizing the solvability (number of events which can give physical solutions normalized by the total number of events analyzed), we can obtain the correct neutralino mass.

Equations to be satisfied are

$$(P_{\tilde{\tau}^\pm} + P_\nu)^2 = m_{\chi^+}^2, \quad (71)$$

$$(P_{\tilde{\tau}^\mp} + \frac{P_{l^\pm}}{z_l})^2 = m_{\chi^0}^2, \quad (72)$$

$$P_\nu^x + \frac{1 - z_l}{z_l} P_{l^\pm}^x = P_{\text{miss}}^x, \quad (73)$$

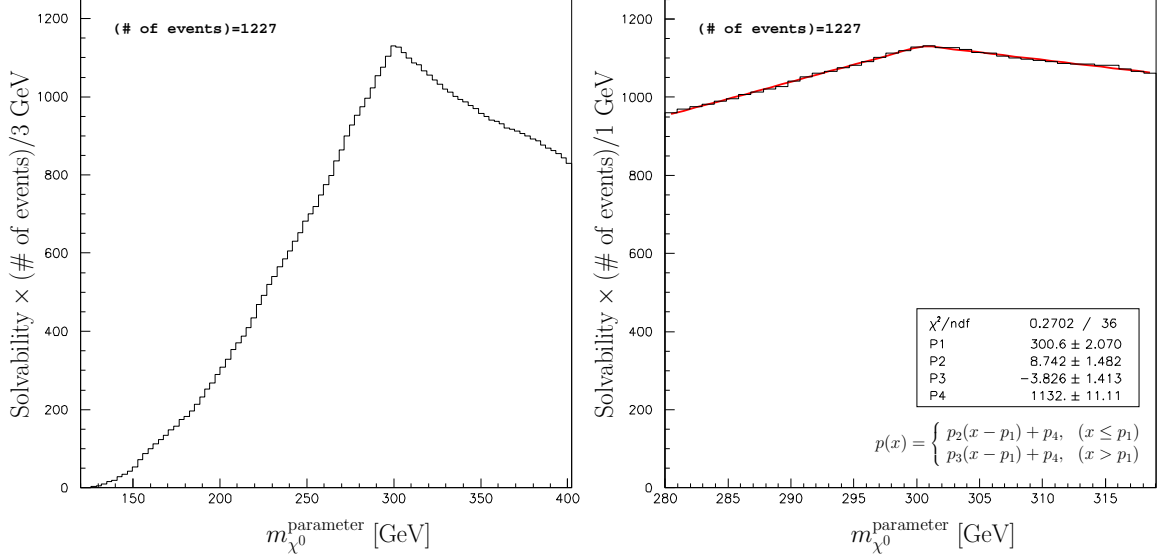


Figure 7: The solvability analysis for the neutralino mass. The right figure shows the solvability near the peak.

$$P_\nu^y + \frac{1 - z_l}{z_l} P_{l^\pm}^y = P_{\text{miss}}^y, \quad (74)$$

whereas there are four unknowns in these equations:

$$P_\nu^x, \quad P_\nu^y, \quad P_\nu^z, \quad z_l. \quad (75)$$

Eq. (72) is a linear equation for  $z_l$  in the approximation of  $m_l = 0$ , and by using the solution, Eqs. (73) and (74) become also linear equations for  $P_\nu^x$  and  $P_\nu^y$ , respectively. Eq. (71), on the other hand, is a quadratic equation for  $P_\nu^z$ , and therefore there can be zero or two real-number solutions. (In general, an equation of this type may have a unique physical solution by the constraint  $E_\nu > 0$ . However, one can show that Eq. (71) always have zero or two solutions by the fact that  $E_{\tilde{\tau}^\pm} > |P_{\tilde{\tau}^\pm}^z|$ .) The number of events should be maximized at the correct neutralino mass when we impose conditions:  $0 \leq z_l \leq 1$  and existence of real-number solutions of Eq. (71).

The number of events with a physical solution is shown in Fig. 7 for various input neutralino masses. It indeed shows a sharp peak at the correct neutralino mass, 300 GeV. We have used the correct value of the chargino mass in the analysis. In the actual situation, the experimental error in the chargino mass will propagate into the error in the peak location. Fitting with two linear functions near the peak, we find that the neutralino mass can be measured quite accurately ( $301 \pm 2$  GeV) if the chargino mass is known.

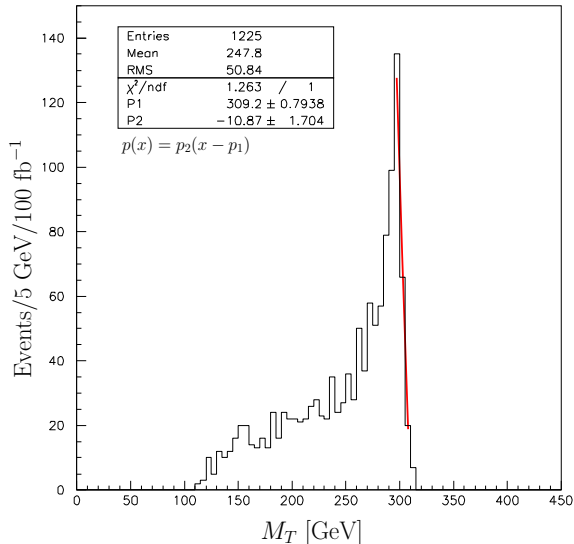


Figure 8: The transverse mass distribution for the chargino mass measurement.

### 6.2.3 Transverse mass analysis for the chargino mass

Once we know the neutralino mass by, for example, the method of the endpoint of the  $M_{\tilde{\tau}\mp l\pm}$  distribution, the transverse momentum of the neutrinos from the chargino decay can be reconstructed without the two-fold ambiguity from Eqs. (72–74). We can then form a transverse mass in Eq. (67) and the chargino mass can be obtained by looking for an endpoint of the distribution.

We show in Fig. 8 the distribution of the transverse mass,  $M_T$ . We can see a sharp peak near the correct chargino mass. The endpoint is again smeared by the resolution of the missing transverse momentum. An appropriate fitting is necessary for the extraction of the chargino mass. For a simple fitting by a linear function, we obtain a significantly larger value ( $309.2 \pm 0.8$  GeV) due to the finite resolution.

### 6.2.4 Solvability analysis for the chargino mass

The solvability analysis can also be done for the chargino mass once we know the neutralino mass. The solvability is plotted in Fig. 9 where we see that the solvability saturates near the chargino mass.

By looking for a point where the solvability saturates, we can obtain the chargino mass ( $303 \pm 1$  GeV).

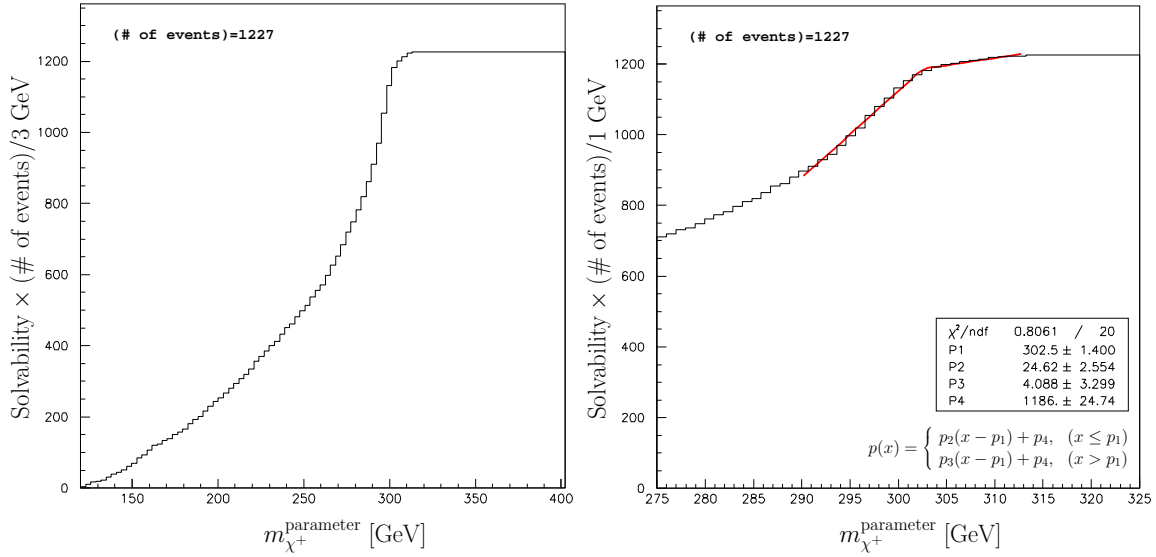


Figure 9: The solvability analysis for the chargino mass measurement. The right figure is the same analysis with a better resolution near the threshold.

### 6.3 Energy and angular distributions

Now we examine whether the energy and angular distributions obtained in Section 4 are visible in actual experiments. Especially, there is always a false solution in the Eqs. (71–74), which may destroy the theoretical distributions. One purpose of this analysis is to understand the effect of the false solution.

In the analysis, we have used the events passed through the selection cut in Eq. (70). We assume in the following that the chargino and neutralino masses are known and ignore errors in the mass measurements.

#### 6.3.1 $z_l$ distribution

This distribution measures the polarization of the  $\tau$  lepton from the neutralino decay. We do not need to distinguish events with different lepton charges since the theoretical distributions are the same (Eq. (40)).

The measurement of the energy fraction of the lepton,  $z_l$ , does not suffer from the two-fold ambiguity since Eq. (72) is a linear equation and we do not need to know  $P_\nu^z$ .

The distribution is shown in Fig. 10. We fit the distributions with the theoretical curve in Eq. (40) by making  $a_N$  a parameter. We obtain  $a_N = 1.1 \pm 0.2$  (solid curve) for  $a_N^{\text{th}} = 1.0$  in this

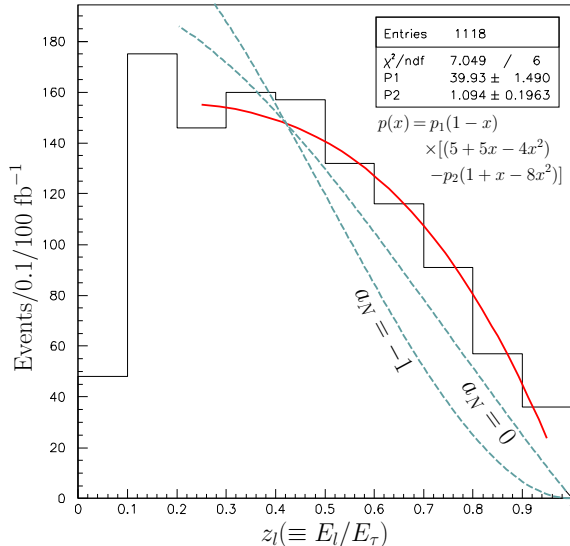


Figure 10: The reconstructed distribution of the lepton-energy fraction ( $z_l$ ). The solid curve is the best fit with a theoretical function in Eq. (40). The curves with  $a_N = 0, -1$  are also shown (dashed curves).

model. Curves with  $a_N = 0$  and  $a_N = -1$  are shown in the figure (dashed lines, we used the same normalization with the solid curve). We can see that the best-fit curve can be discriminated from those models. The region with small  $z_l$  is affected by the  $p_T$  cut on the leptons. We omitted the region from the fitting.

### 6.3.2 $\cos \theta_1$ distribution

This distribution measures the parity asymmetry in the  $\chi^\pm \chi^0$  production process,  $a_W$ , through Eq. (41). The averaged value of  $f_1$  (weighted by the cross section) depends on a selection cut on  $\hat{s}$ . It is an increasing function of  $\hat{s}_{\min}$ , but the number of events rapidly decreases with  $\hat{s}_{\min}$ . In the model we simulated, the cross section falls off as

$$\frac{d\sigma(\hat{s})}{d\sqrt{\hat{s}}} \propto \exp \left[ -4.3 \left( \frac{\sqrt{\hat{s}}}{\text{TeV}} \right) \right]. \quad (76)$$

The averaged value defined by

$$\langle f_1(\sqrt{\hat{s}_{\min}}) \rangle \equiv \frac{\int_{\sqrt{\hat{s}_{\min}}}^{\infty} \frac{d\sigma(\hat{s})}{d\sqrt{\hat{s}}} f_1(\sqrt{\hat{s}}) d\sqrt{\hat{s}}}{\int_{\sqrt{\hat{s}_{\min}}}^{\infty} \frac{d\sigma(\hat{s})}{d\sqrt{\hat{s}}} d\sqrt{\hat{s}}} \quad (77)$$

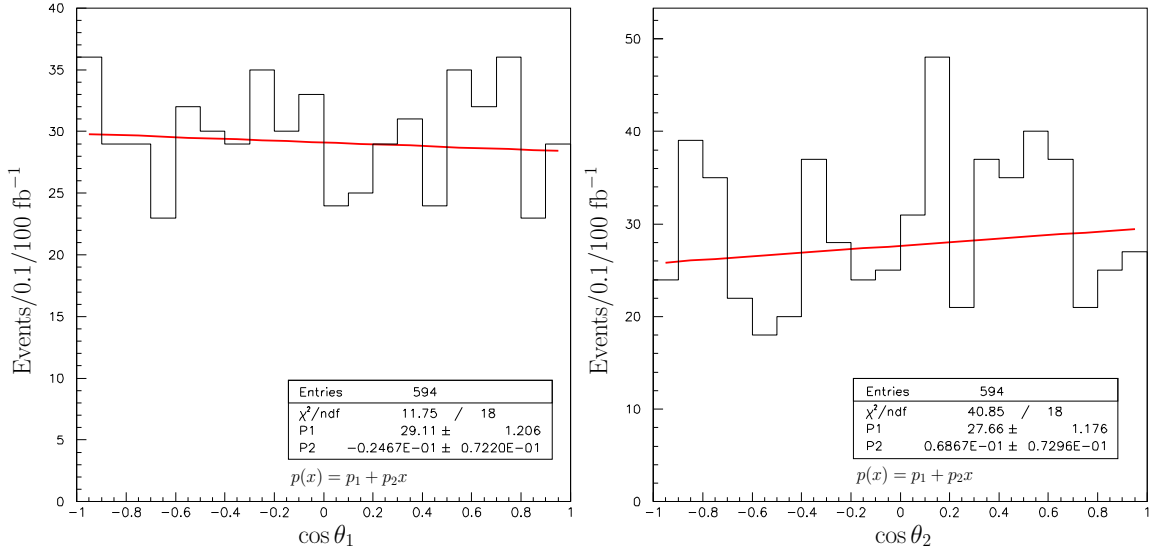


Figure 11: The reconstructed  $\cos \theta_1$  (left) and  $\cos \theta_2$  (right) distributions. The false solutions are included. A selection cut  $\sqrt{\hat{s}} > 900$  GeV is imposed on both of the solutions in each event.

is then estimated to be, for example,

$$\langle f_1(600 \text{ GeV}) \rangle = 0.52, \quad \langle f_1(900 \text{ GeV}) \rangle = 0.74, \quad (78)$$

for  $m_{\chi^+} \simeq m_{\chi^0} \simeq 300$  GeV and  $\xi_W = 1$ . Since the asymmetry will be diluted by false solutions as we see below, it is necessary to impose a cut  $\hat{s}_{\min}$  in order to expect a large asymmetry.

The angle  $\cos \theta_1$  which is defined in the rest frame of the chargino is expressed in terms of the  $\tilde{\tau}^\pm$  energy in the CM frame:

$$\cos \theta_1 = \frac{E_{\tilde{\tau}^\pm}^{\text{CM}} - \gamma_A E_{\tilde{\tau}^\pm}^{(1)}}{\gamma_A \beta_A P_{\tilde{\tau}^\pm}^{(1)}}, \quad (79)$$

where  $\gamma_A$  and  $\beta_A$  are defined in Eq. (8), and  $E_{\tilde{\tau}^\pm}^{(1)}$  and  $P_{\tilde{\tau}^\pm}^{(1)}$  are the energy and momentum in the rest frame of the chargino, respectively. They are given by

$$E_{\tilde{\tau}^\pm}^{(1)} = \frac{m_{\chi^+}^2 + m_{\tilde{\tau}}^2}{2m_{\chi^+}}, \quad P_{\tilde{\tau}^\pm}^{(1)} = \sqrt{\left(E_{\tilde{\tau}^\pm}^{(1)}\right)^2 - m_{\tilde{\tau}}^2}. \quad (80)$$

When we calculate the  $\tilde{\tau}$  energy in the CM frame from the quantities measured in the laboratory frame by boosting to the  $z$ -direction, one encounters the two-fold ambiguity for  $P_\nu^z$  in Eq. (71).

In order not to develop a fake distribution caused by the false solution, we need to be careful when we impose a selection cut on  $\hat{s}$ . We have examined the following three methods of imposing a  $\hat{s}_{\min}$  cut. One is to choose a solution which gives a smaller value of  $\hat{s}$ , and impose a selection cut

$\sqrt{\hat{s}} > 900$  GeV on the chosen event. This strategy effectively picks up the true solution (with the probability of about 63%) because of the distribution in Eq. (76). However, this method causes a bias in the  $\cos \theta_1$  distribution towards larger  $\cos \theta_1$ . For each event, it is likely that the solution with larger  $\cos \theta_1$  (which would mean that the neutrino is emitted to the opposite direction to the chargino in the CM frame) gives a smaller value of  $\hat{s}$ , and thus such a solution is more probable to be chosen. This correlation causes the bias.

The next strategy is to use all the solutions with  $\sqrt{\hat{s}} > 900$  GeV. That is, if we have two solutions which satisfy the cut in an event, we use both solutions. If there is only one solution with  $\sqrt{\hat{s}} > 900$  GeV, we use that one. This strategy causes a fake distribution towards smaller  $\cos \theta_1$  this time. Since we impose a lower cut on  $\hat{s}$ , this strategy tends to select a solution with larger  $\hat{s}$ . By the same reason as above, this tends to pick up a solution with smaller  $\cos \theta_1$ .

The above two lessons lead us to a good strategy to avoid the bias. It is to use both solutions per each event and impose an  $\hat{s}$  cut on *both* of the solutions, i.e., we throw away an event if there is a solution with  $\sqrt{\hat{s}} < 900$  GeV even though it may be a false solution. By doing that, the probability of selecting the true solution is exactly 50%, and there is no obvious reason to expect a fake distribution. We show in Fig. 11 the reconstructed  $\cos \theta_1$  distribution by using the strategy (left figure). A flat distribution is obtained which is expected in this model because  $a_W = 0.0$ . For a more general case, the slope of this distribution should give  $a_W \langle f_1 \rangle / 2$  approximately where the factor of two comes from the effect of false solutions.

### 6.3.3 $\cos \theta_2$ distribution

This measures the product of the parity asymmetries  $a_N$  and  $a_W$  in Eq. (44) through the spin correlation of the neutralino. By the same strategy as in the  $\cos \theta_1$  case, we obtain a flat distribution for  $\cos \theta_2$  as expected. It is shown in the right panel of Fig. 11.

### 6.3.4 $\cos \theta_1 \cos \theta_2$ distribution

Although the  $\cos \theta_1$  and  $\cos \theta_2$  distributions are trivial in this particular model due to  $a_W = 0.0$ , there can be a non-trivial correlation between  $\cos \theta_1$  and  $\cos \theta_2$ . An example is the distribution of the product  $\cos \theta_1 \cos \theta_2$  which measures the product of the parity asymmetries in the neutralino and chargino decays independent of  $a_W$  (see Eq. (47)).

We define a variable,

$$w = h(y) \equiv y(\log |y| - 1), \quad y = \cos \theta_1 \cos \theta_2. \quad (81)$$

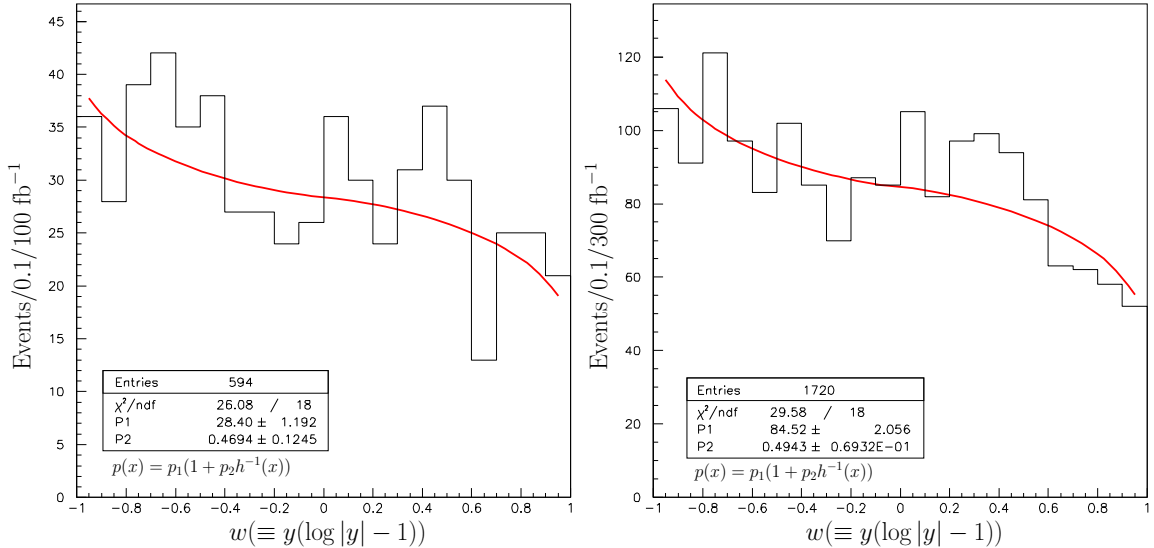


Figure 12: The reconstructed  $w(\equiv \cos \theta_1 \cos \theta_2 (\log |\cos \theta_1 \cos \theta_2| - 1))$  distribution. A deviation from the flat distribution indicates the presence of the spin correlations and parity violation in the chargino and the neutralino decays. The false solutions are included. A selection cut  $\sqrt{\hat{s}} > 900$  GeV is imposed on both of the solutions in each event. The right figure is the same but with  $300 \text{ fb}^{-1}$  of data.

The theoretical distribution in Eq. (47) in terms of the variable  $w$  is

$$d\sigma \propto (1 + a_N \langle f_2 \rangle h^{-1}(w)) dw, \quad (82)$$

where  $h^{-1}$  is the inverse function of  $h(y)$ , i.e.,  $y = h^{-1}(w)$ , and  $-1 \leq w \leq 1$ . The  $w$  distribution is flat in the parity conserving case ( $a_N = 0$ ). The deviation from the flat distribution is a signature of parity violation. The averaged value of  $\langle f_2 \rangle$  depends on  $\sqrt{\hat{s}_{\min}}$ :

$$\langle f_2(600 \text{ GeV}) \rangle = 0.58, \quad \langle f_2(900 \text{ GeV}) \rangle = 0.75. \quad (83)$$

Therefore, with the strategy for the selection cut discussed before, we expect an asymmetry  $a_N \langle f_2 \rangle / 2 \simeq 0.38$  in this model, where the factor of two is the effect of fake solutions.

The reconstructed  $w$  distribution is shown in Fig. 12 where we see deviation from the flat distribution. The right figure is the same analysis with  $300 \text{ fb}^{-1}$  of data. We fit the histogram with the function in Eq. (82) and obtained a significant asymmetry,  $a_N \langle f_2 \rangle / 2 \simeq 0.47 \pm 0.12$  ( $0.49 \pm 0.07$ ) which deviates from zero by  $4\sigma$  ( $7\sigma$ ) with  $100 \text{ fb}^{-1}$  ( $300 \text{ fb}^{-1}$ ) of data. A somewhat larger value compared to the expectation (0.38) can be understood by the fact that the effective  $\sqrt{\hat{s}_{\min}}$  is larger than 900 GeV because we have imposed a cut on both of the solutions.

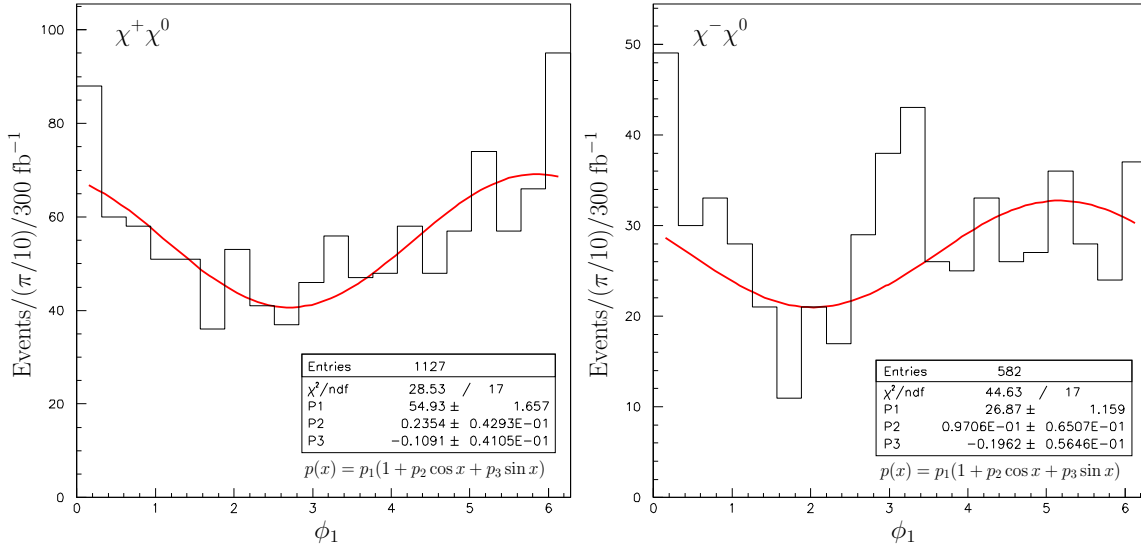


Figure 13: The reconstructed  $\phi_1$  distributions for the  $\chi^+\chi^0$  (left) and the  $\chi^-\chi^0$  (right) production events.

Observation of this distribution together with the measurement of  $a_N$  by the  $z_l$  distribution will be a quite interesting confirmation of the spin correlations.

### 6.3.5 $\phi_1$ distribution

Non-trivial azimuthal-angle distributions show up when there is parity and/or CP violation in the decay vertex. In order to measure this, we need to completely reconstruct the kinematics such as the angle  $\theta$ . The angle  $\phi_1$  is expressed in terms of the angle  $\theta$  and the three-momentum of  $\tau^\pm$  in the CM frame:

$$\tan \phi'_1 = \frac{(P_{\tilde{\tau}}^y)_{\text{CM}}}{(P_{\tilde{\tau}}^x)_{\text{CM}} \cos \theta - (P_{\tilde{\tau}}^z)_{\text{CM}} \sin \theta}, \quad (0 \leq \phi'_1 \leq \pi), \quad (84)$$

with

$$\begin{cases} \phi_1 = \phi'_1 & (\text{if } (P_{\tilde{\tau}}^y)_{\text{CM}} \geq 0) \\ \phi_1 = \phi'_1 + \pi & (\text{if } (P_{\tilde{\tau}}^y)_{\text{CM}} < 0) \end{cases}. \quad (85)$$

In order to define the CM frame in Fig. 1, we need to know the direction of the anti-quark which can be determined only statistically in  $pp$ -collision experiments. We take the  $z$ -direction to be the same direction as that of the total momentum,  $P^z = P_{\chi^\pm}^z + P_{\chi^0}^z$ , in the laboratory frame since the  $\bar{q}$  parton tends to carry a smaller momentum. In order to reduce a number of mis-choices, we impose a cut:  $P^z > 1200 \text{ GeV}$ .

The  $\phi_1$  dependent part of the distribution in Eq. (48) has opposite signs for  $\chi^+$  and  $\chi^-$  productions. We do not impose a cut on  $\hat{s}$  because the  $g_1$  function in Eq. (49) takes its maximum value at the threshold production. (In order to look for a CP asymmetry, it may be better to impose a cut. See Eq. (50).) We also use both solutions for  $P_\nu^z$ . The averaged value of the functions  $g_1$  and  $g_2$  are:

$$\frac{\pi^2}{16}\langle g_1 \rangle = 0.51, \quad \frac{\pi^2}{16}\langle g_2 \rangle = 0.16. \quad (86)$$

We expect that the value will be affected due to the existence of the false solution.

The distributions are shown in Fig. 13 with  $300 \text{ fb}^{-1}$  of data. The left figure is the distribution of the  $\chi^+\chi^0$  events, i.e., the events with a positive-charge lepton, and the right figure is from the  $\chi^-\chi^0$  events. We fit the histogram by a function:

$$p(\phi_1) = p_1(1 + p_2 \cos \phi_1 + p_3 \sin \phi_1). \quad (87)$$

A qualitatively correct behavior is obtained in the  $\chi^+\chi^0$  events, i.e.,  $p_2 > 0$  and  $p_3 = 0$ , but  $\chi^-\chi^0$  events do not show an expected behavior of  $p_2 < 0$  and  $p_3 = 0$  due to poor statistics and the selection cut on  $P^z$ . We can see from the figures that the selection cut on  $P^z$  tends to give a fake distribution peaked near  $\phi_1 \sim 0$  and  $2\pi$  for both  $\chi^+\chi^0$  and  $\chi^-\chi^0$  events. One may be able to avoid this by imposing the  $P^z$  cut on both solutions as we have done in the study of the  $\cos\theta_1$  distribution, but we could not afford the statistics in this model. A looser cut on  $P^z$  results in a fake distribution by the mis-choice of the  $z$ -direction. Nevertheless, it is not a problem for observing a non-trivial distribution since the theoretic distribution is different for  $\chi^+\chi^0$  and  $\chi^-\chi^0$  productions. For example, one can try to rescale the histogram of the  $\chi^-\chi^0$  events and subtract from (or add to) that of the  $\chi^+\chi^0$  events in order to eliminate (or understand) the fake distribution.

### 6.3.6 $\phi_2$ distribution

The  $\phi_2$  distribution can be obtained by the same method. The distribution clearly shows an expected behavior in Eq. (52) with  $a_N = 1.0$  and  $\eta_W = 0.0$ .

## 7 Summary

If  $\tilde{\tau}$  is the lightest among the superpartners of the Standard Model particles, the SUSY signatures at the LHC experiments will be very different from the stable neutralino scenario. We have demonstrated that the production processes of the neutralinos and charginos have rich information on model parameters. The spin correlations of intermediate particles give rise to interesting

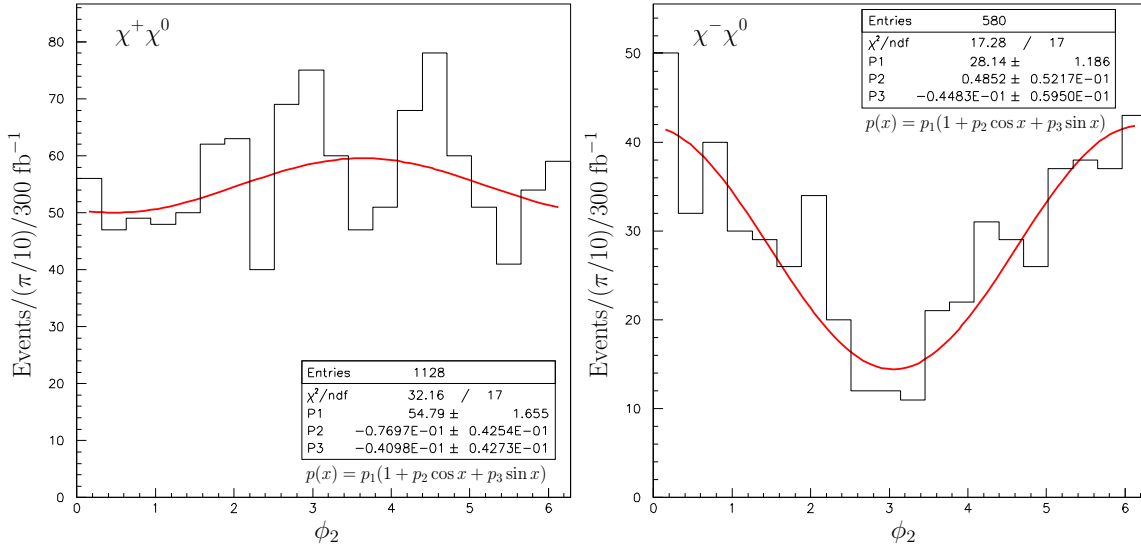


Figure 14: The reconstructed  $\phi_2$  distributions for the  $\chi^+\chi^0$  (left) and the  $\chi^-\chi^0$  (right) production events.

non-trivial distributions in various kinematic variables. In a study of SUSY models at hadron colliders, the productions of neutralinos and charginos have been usually thought of good processes for discovery of SUSY through multi-lepton final states. In the stable neutralino scenario it is nevertheless challenging to extract information on models out of those processes because of the small cross sections and difficult kinematics due to escaping neutralinos. Much attention has been paid to production processes of colored superparticles and their cascade decays for the measurements of the model parameters. However, as we have shown, the chargino-neutralino production process may provide us with the best opportunity for understanding of SUSY models in the long-lived  $\tilde{\tau}$  scenario.

The study presented in this paper is not fully realistic in several senses. We have not included the momentum resolution of the  $\tilde{\tau}$  tracks or efficiency of the identification. Also, in the study of various distributions, we have ignored errors in the measurements of the chargino and the neutralino masses. We have used the transverse missing momentum evaluated by the fast detector simulator, but the resolution may be very different in real experiments. The trigger efficiency of the process has also been ignored. A more detailed analysis is necessary when we discover the long-lived  $\tilde{\tau}$ . The analytical formulae presented in this paper will be useful in such future studies.

This work is inspired by studies of the electroweak theory in Refs. [25] where the differential cross section of the process  $e^+e^- \rightarrow W^+W^-$  is calculated with keeping spin correlations. The various distributions are studied for the confirmation of the  $SU(2)_L \times U(1)_Y$  gauge interaction.

The density matrix calculated there has been used to put constraints on anomalous interactions among gauge bosons at the LEP-II experiments [26]. If  $\tilde{\tau}$  is long-lived, the cross-section formula calculated in this paper can be used as a good test of SUSY at the LHC experiments just like we have confirmed the Standard Model at the LEP experiments.

We here comment on the  $\chi^0\chi^0$  production processes which we did not study in this paper. In many cases, these processes have smaller cross sections than the  $\chi^\pm\chi^0$  process. Since the  $Z$ -boson vertices to the same mass eigenstates,  $Z - \chi_i^0 - \chi_i^0$ , vanish identically, the main production process is  $\chi_i^0\chi_j^0$  with  $i \neq j$ . If we require the opposite charges for two  $\tilde{\tau}$ 's and the leptonic decays for both of the  $\tau$  leptons, the number of events will get further small. However, for the reconstruction of the kinematics, it is much simpler than the  $\chi^\pm\chi^0$  productions. We can reconstruct the final state without the knowledge of the neutralino masses. There is no discrete ambiguity for the reconstruction. The study of these processes will also be important if  $\tilde{\tau}$  is long-lived, although it may be challenging due to the limited statistics.

## Acknowledgments

I thank Alex Friedland and Michael Graesser for discussions and useful comments.

## References

- [1] M. Pospelov, Phys. Rev. Lett. **98**, 231301 (2007) [arXiv:hep-ph/0605215]; K. Kohri and F. Takayama, Phys. Rev. D **76**, 063507 (2007) [arXiv:hep-ph/0605243]; M. Kawasaki, K. Kohri and T. Moroi, Phys. Lett. B **649**, 436 (2007) [arXiv:hep-ph/0703122]; J. Pradler and F. D. Steffen, arXiv:0710.2213 [hep-ph]; K. Jedamzik, JCAP **0803**, 008 (2008) [arXiv:0710.5153 [hep-ph]]; M. Kawasaki, K. Kohri, T. Moroi and A. Yotsuyanagi, arXiv:0804.3745 [hep-ph].
- [2] M. Ibe and R. Kitano, JHEP **0708**, 016 (2007) [arXiv:0705.3686 [hep-ph]].
- [3] I. Hinchliffe and F. E. Paige, Phys. Rev. D **60**, 095002 (1999) [arXiv:hep-ph/9812233].
- [4] J. R. Ellis, A. R. Raklev and O. K. Oye, JHEP **0610**, 061 (2006) [arXiv:hep-ph/0607261].
- [5] G. Polesello and A. Rimoldi, ATLAS Internal Note ATL-MUON-99-006.
- [6] S. Ambrosanio, B. Mele, S. Petrarca, G. Polesello and A. Rimoldi, JHEP **0101**, 014 (2001) [arXiv:hep-ph/0010081].

- [7] W. Buchmuller, K. Hamaguchi, M. Ratz and T. Yanagida, Phys. Lett. B **588**, 90 (2004) [arXiv:hep-ph/0402179].
- [8] K. Hamaguchi, Y. Kuno, T. Nakaya and M. M. Nojiri, Phys. Rev. D **70**, 115007 (2004) [arXiv:hep-ph/0409248].
- [9] J. L. Feng and B. T. Smith, Phys. Rev. D **71**, 015004 (2005) [Erratum-ibid. D **71**, 019904 (2005)] [arXiv:hep-ph/0409278].
- [10] A. Rajaraman and B. T. Smith, Phys. Rev. D **76**, 115004 (2007) [arXiv:0708.3100 [hep-ph]].
- [11] V. D. Barger, R. W. Robinett, W. Y. Keung and R. J. N. Phillips, Phys. Lett. B **131**, 372 (1983).
- [12] H. E. Haber, arXiv:hep-ph/9405376.
- [13] B. K. Bullock, K. Hagiwara and A. D. Martin, Nucl. Phys. B **395**, 499 (1993).
- [14] M. R. Buckley, H. Murayama, W. Klemm and V. Rentschler, arXiv:0711.0364 [hep-ph].
- [15] G. Corcella *et al.*, arXiv:hep-ph/0210213.
- [16] P. Richardson, JHEP **0111**, 029 (2001) [arXiv:hep-ph/0110108].
- [17] S. Moretti, K. Odagiri, P. Richardson, M. H. Seymour and B. R. Webber, JHEP **0204**, 028 (2002) [arXiv:hep-ph/0204123].
- [18] H. L. Lai *et al.* [CTEQ Collaboration], Eur. Phys. J. C **12**, 375 (2000) [arXiv:hep-ph/9903282].
- [19] S. Jadach, Z. Was, R. Decker and J. H. Kuhn, Comput. Phys. Commun. **76**, 361 (1993).
- [20] E. Richter-Was, arXiv:hep-ph/0207355.
- [21] C. G. Lester and D. J. Summers, Phys. Lett. B **463**, 99 (1999) [arXiv:hep-ph/9906349].
- [22] K. Kawagoe, M. M. Nojiri and G. Polesello, Phys. Rev. D **71**, 035008 (2005) [arXiv:hep-ph/0410160].
- [23] H. C. Cheng, J. F. Gunion, Z. Han, G. Marandella and B. McElrath, JHEP **0712**, 076 (2007) [arXiv:0707.0030 [hep-ph]].
- [24] M. Davids *et al.*, CMS Note 2006/077.

- [25] K. J. F. Gaemers and G. J. Gounaris, *Z. Phys. C* **1**, 259 (1979); K. Hagiwara, R. D. Peccei, D. Zeppenfeld and K. Hikasa, *Nucl. Phys. B* **282**, 253 (1987); P. Mery, M. Perrottet and F. M. Renard, *Z. Phys. C* **36**, 249 (1987); M. S. Bilenky, J. L. Kneur, F. M. Renard and D. Schildknecht, *Nucl. Phys. B* **409**, 22 (1993).
- [26] P. Abreu *et al.* [DELPHI Collaboration], *Phys. Lett. B* **502** (2001) 9 [arXiv:hep-ex/0102041]; P. Achard *et al.* [L3 Collaboration], *Phys. Lett. B* **586**, 151 (2004) [arXiv:hep-ex/0402036]; S. Schael *et al.* [ALEPH Collaboration], *Phys. Lett. B* **614** (2005) 7; J. Abdallah *et al.* [DELPHI Collaboration], *Eur. Phys. J. C* **54**, 345 (2008) [arXiv:0801.1235 [hep-ex]].